Journal of Maps

ISSN: (Print) 1744-5647 (Online) Journal homepage: http://www.tandfonline.com/loi/tjom20

Structural glaciology of Isunguata Sermia, West Greenland

Christine Jones, Jonathan Ryan, Tom Holt & Alun Hubbard

To cite this article: Christine Jones, Jonathan Ryan, Tom Holt & Alun Hubbard (2018) Structural glaciology of Isunguata Sermia, West Greenland, Journal of Maps, 14:2, 517-527, DOI: 10.1080/17445647.2018.1507952

To link to this article: https://doi.org/10.1080/17445647.2018.1507952

JOURNAL OF MAPS
2018, VOL. 14, NO. 2, 517–527
https://doi.org/10.1080/17445647.2018.1507952

Taylor & Francis
Taylor & Francis Group

Science

Structural glaciology of Isunguata Sermia, West Greenland

Christine Jones[a], Jonathan Ryan[a], Tom Holt[a] and Alun Hubbard[b]

[a]Geography and Earth Sciences, Aberystwyth University, Aberystwyth, UK; [b]Centre for Arctic Gas Hydrate, Environment and Climate, UiT – The Arctic University of Norway, Department of Geology, Tromsø, Norway

ABSTRACT

We present a 1:42,000 scale map of Isunguata Sermia, a land-terminating outlet glacier draining the western-sector of the Greenland Ice Sheet. Structure-from-Motion software applied to ~3,600 aerial images collected by a fixed-wing unmanned aerial vehicle in July 2015 allowed us to produce a high resolution (0.3 m ground sampling distance (GSD)) orthomosaic and digital elevation model (DEM; 1.5 m GSD).These products were used to map and describe the structural, geomorphological and hydrological features of the lower 16 km terminus of Isunguata Sermia and include many thousands of crevasses, crevasse traces and supraglacial channels. Additionally, several geomorphological features and pro-glacial hydrological features were identified, including debris-covered ice, lateral moraines and ice-marginal lakes. The map has potential for informing and reconstructing the long-term dynamic history of the glacier, including its response to variable environmental forcing.

ARTICLE HISTORY
Received 13 April 2017
Revised 15 October 2017
Accepted 31 July 2018

KEYWORDS
Greenland Ice Sheet; structural glaciology; crevasses; supraglacial hydrology; ice flow

1. Introduction

The structures found on glaciers, ice sheets and ice shelves provide information regarding past and present patterns of ice flow, as well as insights into the associated mechanical processes and properties of ice (Benn & Evans, 2010; Hulbe, LeDoux, & Cruikshank, 2010). Primary structures such as stratification from annual snow layers, ice lenses and unconformities form mostly in the accumulation zone, and deform as they advect downstream towards the terminus. Secondary structures, resulting directly from ice flow and cumulative strain, express themselves as both brittle and ductile features. Brittle features include faulting and crevasses (Hambrey & Muller, 1978), whereas ductile features include healed crevasse traces and foliation (Hambrey & Lawson, 2000). Both primary and secondary structures develop and evolve down-glacier as an expression of their cumulative strain history, and are commonly observed across the ice surface as relict or inherited features. Mapping such features, and determining their interrelationships, is useful for understanding their response to variable environmental forcing via the reconstruction of the long-term dynamic history of an ice mass.

Recent technological advances in autopilot hardware and firmware have allowed researchers to carry out unmanned aerial vehicle (UAV) surveys at relatively low-costs. UAVs are beneficial to the field of glaciology due to their ease of deployment and user-based control over the equipment, sensors and survey area. Typically, UAVs are mounted with digital cameras to collect high resolution imagery of the fieldsite. The spatial coverage, as well as the desired camera resolution and survey timing, are dictated by the user, with overlapping images being acquired by the UAV to produce fine (sub-centimetre) three-dimensional models and orthorectified image mosaics of study sites using Structure-from-Motion (SfM) photogrammetry (Smith, Carrivick, & Quincey, 2015). Hence, there has been a steady rise in the deployment of UAVs to investigate glacier processes (i.e. Rippin, Pomfret, & King, 2015; Ryan et al., 2015; Ryan, Hubbard, Stibal, Box, & Team., D. S. P., 2016). For more information on UAV application in glaciology, see the recent review by Bhardwaj, Sam, Martín-torres, and Kumar (2016).

Here, we pioneer the use of high resolution aerial imagery acquired by a fixed wing UAV to investigate the structural glaciology of Isunguata Sermia (IGS), a 1500 km^2 land-terminating outlet glacier draining the western-sector of the GrIS. The specific aim of this study is twofold: (1) to provide a full structural representation of the terminus of IGS, and, (2) to further highlight the potential of UAV imagery for informing structural glaciological studies. In July 2015, over 245 km of UAV surveying was acquired over the terminus of IGS, yielding 4924 geo-tagged aerial images with a ground resolution equivalent to 30 cm. These images were used to generate a georeferenced orthomosaic and digital elevation model (DEM) with an absolute horizontal and vertical accuracy of 5 and 8 m, respectively for both the orthomosiac and the DEM. From these products, the primary and secondary structural features were mapped alongside geomorphological and hydrological features (Figure 1). All mapped features can be seen within the Main Map supplemented alongside this paper.

CONTACT Christine Jones cs_jones@outlook.com Geography and Earth Sciences, Aberystwyth University, Aberystwyth, UK

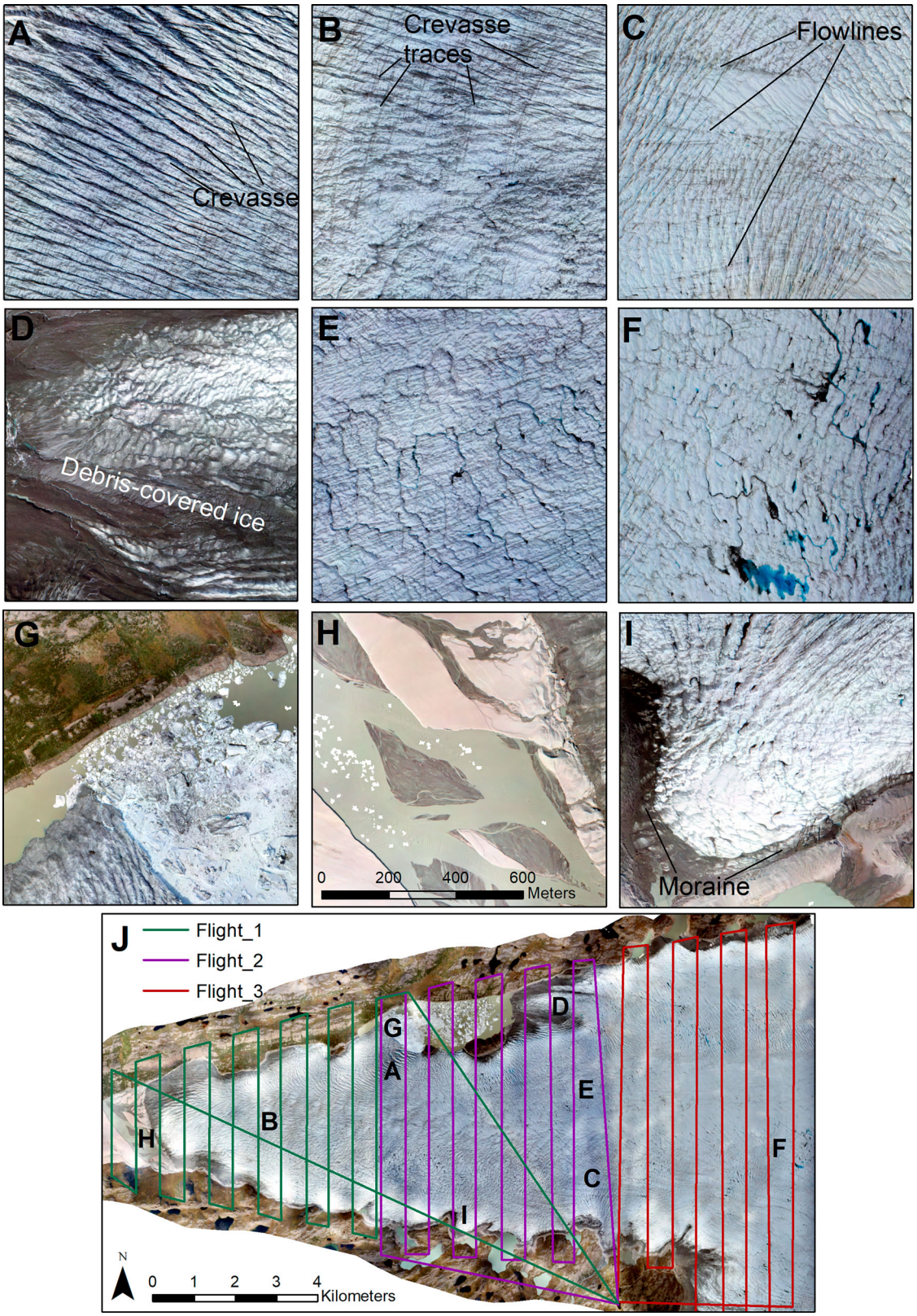

Figure 1. Feature identification in the UAV orthomosiac, as discussed in the main text. (A) crevasses, (B) crevasse traces, (C) longitudinal flowlines, (D) debris-covered ice, (E) supraglacial channels, (F) supraglacial lakes, (G) marginal lakes, (H) outwash plain, (I) moraine, (J) Overview map of the locations of features A-I, with the flight paths of the UAV also illustrated. Scale on insert H is applicable to all inserts. The difference between the appearance of crevasses and crevasse traces is highlighted in Sections 5.1.2 and 5.1.3.

2. Study site

IGS is one of the land-terminating outlet glaciers that drain the western sector of the GrIS within the Arctic circle (Figure 2). This section of the GrIS is characterized by high ablation rates and low accumulation, which combine to produce the highest estimated equilibrium line altitude (ELA) on the GrIS of 1553 m (Meierbachtol, Harper, & Johnson, 2016). The total

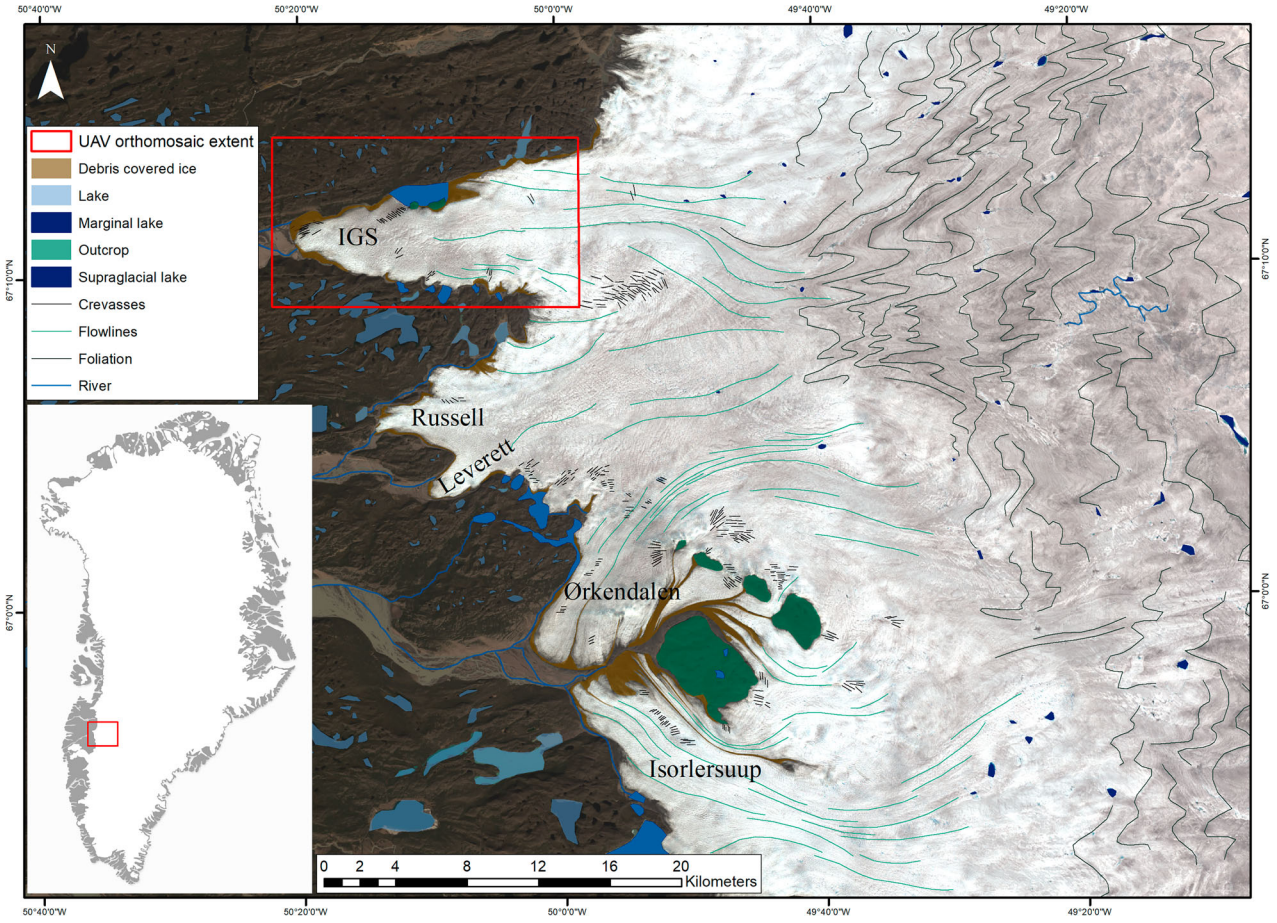

Figure 2. Location of Isunguaga Sermia (IGS) within the Kangerlussuaq region of the western sector of the GrIS. The neighbouring glaciers of Russell, Leverett, Ørkendalen and Isorlersuup have not been considered in this study, however the extent of the structural features as seen from 30 m Landsat 8 imagery have been digitized within this figure to highlight the lower degree of detail obtained for structural mapping from Landsat imagery. IGS has been the focus of numerous scientific research due to a combination of its ease of access and location away from marine influences, meaning that all changes within the glacial ice dynamics are solely attributed to surface melt forcing (Fitzpatrick et al., 2013).

area of the IGS drainage basin from the ice flow divide is 15,900 km^2, with the glacier terminating within a deep bedrock trough. This trough extends ~20 km upglacier and has a primary influence on ice flow and subglacial hydrology (Lindbäck et al., 2015). Ice thickness varies from <100 m at terminus to around 800 m some 45 km from the terminus, with thickness increasing to >1500 m 100 km inland (Lindbäck et al., 2014). Borehole thermistor measurements reveal that englacial ice with temperatures down to −12°C is advected into IGS from the ice sheet interior. These measurements, coupled with modelling, also confirm the presence of a temperate basal ice layer at IGS. This temperate basal ice layer increases in thickness from 3% (~20 m) of the ice column height 45.5 km inland to 100% at the terminus (Harrington, Humphrey, & Harper, 2015).

3. Data, methods and software

3.1. UAV platform

The UAV used in this study is a custom-built Skywalker X8, identical to that used in Ryan et al. (2015, 2016). The UAV is constructed from expanded polypropylene foam, has a wingspan of 2.1 m and is powered by a 26 Ah, 14.4 V Lithium-Ion battery pack. In this configuration the UAV has an all-up weight of about 4 kg and a range of up to 100 km. A PixHawk autopilot, that utilizes a compass, a three-axis accelerometer, a barometer and a uBlox NEO-7 GPS, provides the UAV with autonomous control to follow a pre-programmed flight path, although it was manually launched and landed. The UAV is fitted with a 16.1 MPix Sony NEX-5N digital camera and set to capture imagery in RAW mode with a fixed shutter speed, ISO and aperture of 1/1000 s, 100 and 8, respectively. The camera was programmed to take an image every 50 m of horizontal distance travelled and each image was tagged with the GPS and attitude information recorded by the autopilot. Geolocation accuracy of the images is dependent on the accuracy of the UAV's L1 GPS, which is around 15 m. All imagery was collected from nadir with the exception of a few images at the edge of the survey grid when the UAV banked towards the next waypoint. Due to the scale of the area covered by the UAV flightpaths, it was not possible to set out ground control points during the UAV surveying.

3.2. Mission planning

The UAV was programmed to fly three gridded flight patterns over the lower 16 km ablation area of IGS on 12 July 2015 at an altitude of 800 m. Flights were planned using the open-source Mission Planner software (http://ardupilot.org/planner/docs/mission-planner-overview.html). The ground resolution of the UAV imagery varied from 10 to 20 cm because although the UAV maintained a constant height above sea-level, the glacier surface elevation ranged between 18 and 81 m a.s.l. To ensure that the resulting imagery could be accurately co-registered to one another a side overlap of 40–50% was maintained between the survey profiles. Each survey was 80 km in length and took the UAV just over one hour in duration, with a total of 4924 images acquired.

3.3. Three-dimensional model generation

A single georectified orthomosaic and associated DEM were derived from 3637 of the images acquired using Agisoft PhotoScan. To do so, we followed a well-established structure-from-motion processing routine in Agisoft PhotoScan (Version 1.2.5): further details of which can be found in Tonkin, Midgley, Graham, & Labadz, 2014; Ryan et al., 2015, 2017; Gindraux, Boesch, & Farinotti, 2016; Thomson & Copland, 2016. Following the above mentioned methods, 701,762 tie-points and 10,871,869 pixel projections were created in Agisoft Photoscan between the individual images using the image GPS and altitude tag. This ensured maximum image overlap and accurate georeferencing of the resulting products. The resulting DEM has a point density of 0.76 points per square metre, whilst both the orthomosiac and DEM have a final reprojection error of 1.05 px (equivalent to 30.03 cm) as reported by the processing report created in Agisoft Photoscan. The orthomosaic and DEM had original pixel resolutions of 0.28 and 1.43 m, respectively, and were subsequently resampled to 0.5 and 1.5 m.

3.4. Accuracy and RMS errors

Twenty-five randomly distributed points over the stable off-glacier terrain (boulders, road, etc.) were located throughout the UAV photogrammetric products to be used as tie-points to accurately determine the root-mean-squared difference (RMSD) errors of the products within a real-world spatial context. We assess the vertical accuracy of our UAV DEM by comparison with the Greenland Ice Mapping Project (GIMP) DEM (Howat, Negrete, & Smith, 2014). The two products compare with a RMSD of 8 m and do not show a trend in any direction. We assessed the UAV photogrammetric horizontal errors using a set of fixed bedrock check points obtained from Google Earth imagery, which has an accuracy of 1.59 m (Mohammed, Ghazi, & Mustafa, 2013). The check points have an RMSD of 5 m when compared to the UAV orthomosaic.

3.5. Velocity flow field

A surface velocity flow field of IGS was derived using cross-correlation feature tracking of a pair of Landsat 8 images from 8 July 2015 (and 8 July 2016 (Figure 3) (scene ID of 8 July 2015: LC08_L1TP_007013_20150708_20170407_01_T1; scene ID of 8 July 2016: LC08_L1TP_009013_20160708_20170323_01_T1). Feature tracking was undertaken in MATLAB using the ImGRAFT toolbox (Messerli & Grinsted, 2015; available from http://imgraft.glaciology.net/home). The flow field aided the interpretation of mapped structural features and shows that IGS has a velocity of between 0.05 and 0.90 ± 0.2 m d^{-1} (18–328 m yr^{-1}), with the average velocity along the center of the glacier of 0.26 ± 0.2 m d^{-1} (95 m yr^{-1}).

4. Description of glaciological features and structural glaciology

4.1. Glaciological features

4.1.1. Glacier extent

Since no UAV imagery was captured of the upper extent of IGS, the extent of the structural mapping covers an area of 115 km^2 extending 19 km inland from the glacier terminus. The orthomosiac provides sufficient detail to map the lower extent of IGS, due to the spectral contrast between the ice surface and surrounding terrain. Initially, in areas of heavy debris-cover, where the contrast is lower, the DEM was used to distinguish between debris-covered ice (gently sloping surface) and the lateral moraines (steep-sided).

4.1.2. Crevasses

Crevasses range in width from several millimetres to many decimetres and there are a few crevasses that are up to 100 m wide (Colgan et al., 2016; Holdsworth, 1969). Crevasses form on glaciers once the critical conditions of the net strain accumulation have reached the ice surface (Vaughan, 1993), with the crevasses orientated perpendicular to the direction of the primary tensile force (Hubbard, Blatter, Nienow, Mair, & Hubbard, 1998; Van der Veen, 1999). The changing pattern and orientation of crevasses provides insights into cumulative stress and strain history, particularly in the proliferation of principal stresses (Vornberger & Whillans, 1986, 1990).

Across the tongue of IGS, crevasses and fractures are the dominant surface structure, with over 21,000 mapped. The limit of the mapped crevasse size, given

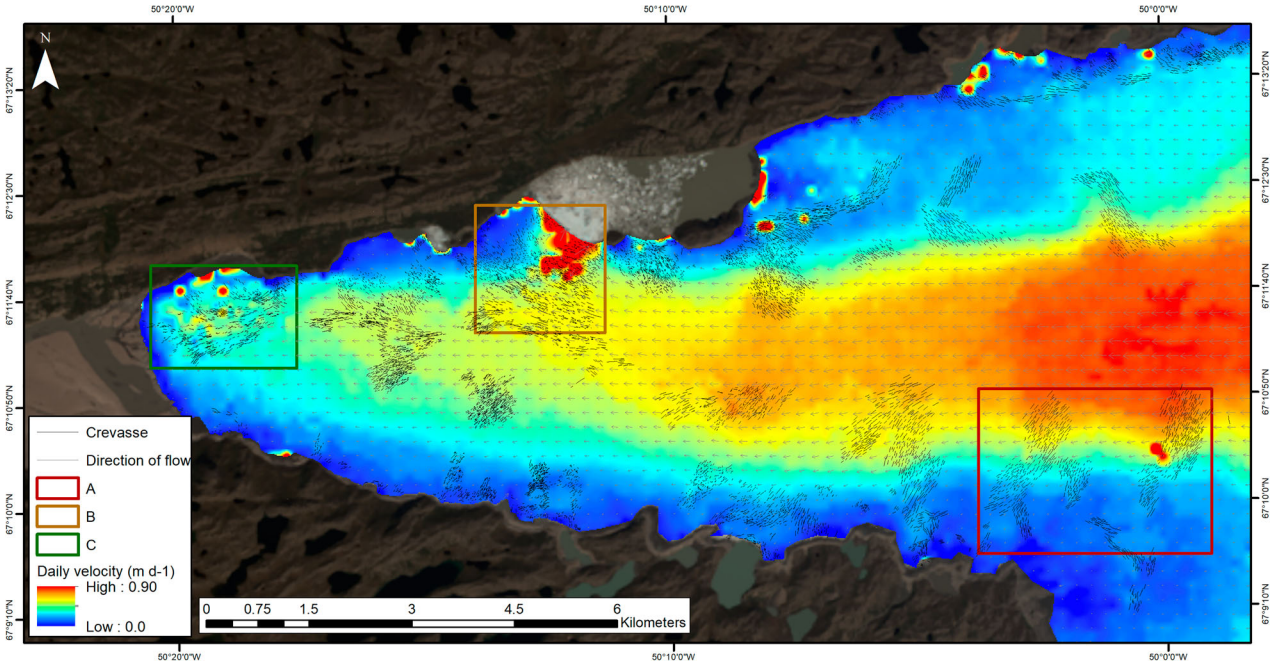

Figure 3. Isunguata Sermia daily velocity flow field, obtained through numerical cross-correlation feature tracking of two Landsat 8 images; 8 July 2015 and 8 July 2016 (scene ID of 8 July 2015: LC08_L1TP_007013_20150708_20170407_01_T1; scene ID of 8 July 2016: LC08_L1TP_009013_20160708_20170323_01_T1). Crevasses play an important role in regulating surface ablation (Cathles, Abbot, Bassis, & MacAyeal, 2011), meltwater retention and drainage (Forster et al., 2014) and, consequently, glacier velocity through basal sliding. The digitization of the crevasses have therefore been overlaid to demonstrate the relationship between crevasse orientation and the changing direction and velocity of the glacier flow field. Boxes A–C are discussed within Section 5.1.2. Background image: Landsat 8 image, acquired on 8 July 2015.

the resolution of the imagery, is ~1 m in width. Crevasses were mapped as both polyline and polygon shape files, with their width being assessed via the 'measure tool'; crevasses ≤3 m in width were mapped as polyline, whilst crevasses >3 m in width were mapped as polygons. Whilst the manual mapping of features was accurate and allowed the production of a good quality product, it was also time-consuming. Attempts were made to automate the mapping of crevasses by searching for troughs in the DEM, but they proved unsuccessful because the process was sensitive to the value of the threshold and smaller, linear cracks were not detected. Automated mapping procedures from high resolution imagery are, however, advancing (e.g. Yang et al., 2015) and future studies may be able to incorporate these techniques for crevasse mapping.

The distribution of crevasses is informative of surface strain rates and the velocity field, with most crevasses concentrated towards the margins of the glacier, and with a lower density of crevasses identified along the central flow unit. The observed pattern of crevassing also varies considerably longitudinally along the length of the glacier tongue; within the upper reaches, crevasses are primarily clustered in groups of 150 per km^2 and predominantly orientated at a 45-degree angle to the direction of ice flow towards the center of the glacier and rotate to become perpendicular to ice flow at the (south) glacier margin (Figure 3 – box A) (these crevasses are defined as 'longitudinal'). Down glacier, the pattern of crevassing is influenced by the presence of ice-marginal lakes, particularly at the large ice-marginal lake on the northern margin of IGS. Here, transverse crevasses cross-cut one another with an average length of 15 m, average width of ~3 m and average density of ~700 crevasses per km^2 (Figure 3 – box B). The northern margin of the glacier terminus is dominated by the presence of over 1500 longitudinal crevasses which have a mean length of 44 m and density of ~400 crevasse per km^2 (Figure 3 – box C).

4.1.3. Crevasse traces

Traces form when a fracture or crevasse subsequently heals as it advects from a tensile zone of strain to a compressive one or with a change in orientation of principal stress. These conditions are commonly found towards the land-terminus of the glacier where it is generally thinning and slowing. When a crevasse closes and heals, a distinct trace can be observed due to the infilling of the former crevasse with a combination of snow, debris or refrozen meltwater. Goodsell, Hambrey, and Glasser (2002) determined that crevasse traces normally appear as coarse-grain recrystallized blue ice, though they can also take a firn-like appearance at the ice surface and are observed as white lineations with granular infills.

Crevasse traces are apparent along the entire length of IGS and are predominantly observed as recrystallized blue ice. These features follow no overriding pattern or orientation, vary in length from 7 to 680 m with

a mean length of ~100 m and commonly intersect with areas of active crevassing. Detectable crevasse traces are mapped as polylines and are limited to features that have a width of >1 m due to the resolution of the imagery.

4.1.4. Flowlines

Longitudinal flowlines are three-dimensional longitudinal structures that commonly occur parallel to the margins of individual flow units (Glasser, Jennings, Hambrey, & Hubbard, 2015). They are detected across the glacier surface as a dark lineation with their total length being determined by ice velocity in respect to the distance it takes the feature to be lost due to strain compression and direction down-glacier (Holt, Glasser, Quincey, & Siegfried, 2013). Glasser and Gudmundsson (2012) determined three possible key mechanisms to explain their formation: (1) When ice flows from a wide accumulation basin into a marginally constrained narrow tongue, longitudinal flowlines form due to net lateral compression. (2) They form at the shear margin between separate flow units occurring when two glacier tributaries flowing at different velocities, converge together. (3) They are the surface expression of subglacial bed perturbations formed in zones of fast-flow with rapid basal sliding such as ice-streams.

At IGS, 23 prominent longitudinal flowlines are identified within the upper reaches of the tongue (Figure 4). Without further geophysical investigation we cannot be entirely sure of their formation mechanism but it is likely, given the topographic setting of IGS and the extrusive flow regimen, that they are due to extreme lateral compression – mechanism 1 as identified by Glasser and Gudmundsson (2012) above.

4.1.5. Debris-covered ice

Supraglacial debris is recognized by a distinct dark brown and/or grey surface. At IGS, debris-covered ice has a net total area of 8.5 km^2 and is largely observed along the lateral margins and at the terminus. This is typical of a glacial environment, where glacier recession can expose the valley sides and destabilize lateral moraines, which consequently increases the volume of material deposited on the glacier surface through mass movement (Nakawo, Iwata, & Yoshida, 1986) or aeolian processes (Oerlemans, Giesen, & Van Den Broeke, 2009). However, these mechanisms are not necessarily dominant at IGS, with previous research on the neighbouring Russell glacier suggesting that debris supplied to the ice surface is largely derived from the basal ice layer, with an insignificant contribution from supraglacial and englacial routes (Adam & Knight, 2003). As IGS has a similar bed topography and composition to Russell Glacier, the same mechanisms creating debris-covered ice can be applied to both sites. It is therefore proposed that the debris-covered ice at IGS is an accumulation of sediment from subglacial erosion that is exposed due to the ongoing melting of the basal ice layer at the glacier margins.

4.2. Geomorphological features

4.2.1. Moraine

Distinct suites of lateral moraines are observed along the margins of IGS, and can be found intermittently along its entire length. Lateral moraines typically comprise a mix of glacial debris that have been eroded, entrained, transported and deposited by the glacier. At IGS, there are no distinct nunataks or aerial rock exposures apparent up-glacier (Figure 2), hence we presume that the sediment and debris is of subglacial origin. The lateral moraines mapped have a width of 80–100 m and are constrained by the glacier and valley walls.

Both the velocity flow field and UAV-derived DEM were used to distinguish between debris-covered ice and moraine features, with areas of debris-covered ice having a minimum velocity of 0.05 m d^{-1}, whereas areas deemed to be moraine exhibited no signs of movement. The DEM supported this by showing a difference in height between the two features, with moraines generally being ~6 m lower than areas of debris-covered ice.

4.3. Hydrological features

4.3.1. Supraglacial channels

The UAV survey was undertaken during the peak of the melt season, so it is presumed that the products are an accurate representation of the maximum extent of the supraglacial meltwater network. Supraglacial channels develop seasonally across the ablation area of the GrIS, with meltwater collecting in depressions which act as natural low points for supraglacial water to pool within. Channels are then formed by surface meltwater down-cutting into the glacier surface. Channels experience changes to their dimensions, capacity and meandering characteristics due to thermal and radiative processes (Alexander, Davies, & Shulmeister, 2011).

Marston (1983) found that meandering channels occur in areas where channel down-cutting proceeds at rates twice that of ablation, whereas the occurrence of straight channel segments are largely influenced by the surface relief and the density and orientation of crevasses. We have no ablation rates for IGS, however the lower ablation zone of IGS corresponds in ice elevation and structural dynamics to the neighbouring Russel Glacier, which has an annual-mean ablation rate of ~4.3 m ice equivalent (van As et al., 2012). Due to the similar size and topographical constraints of the two glaciers, it is assumed that IGS has a similar ablation rate to Russell Glacier. At

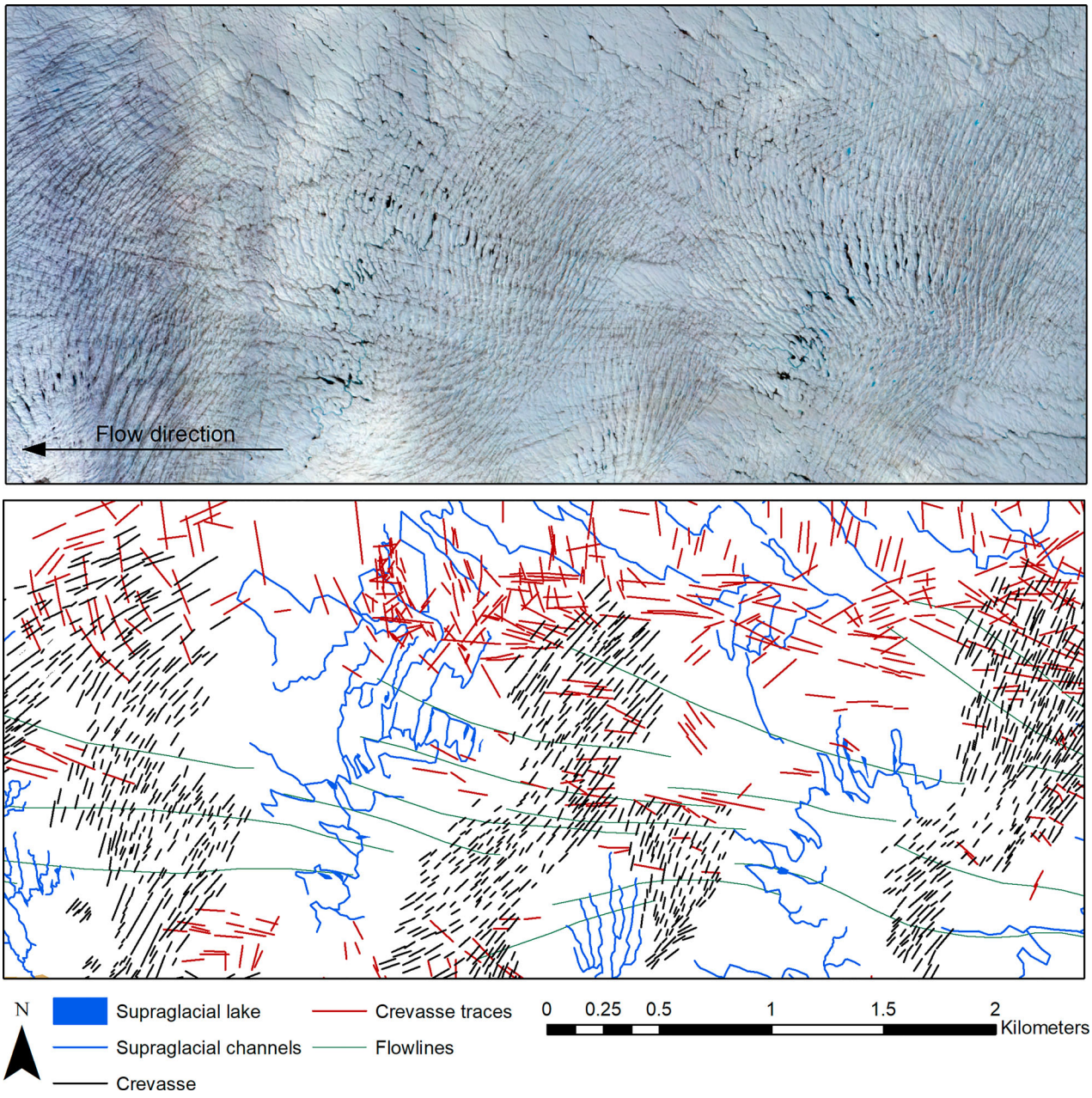

Figure 4. Digitization of the longitudinal flowlines evident throughout Isunguata Sermia. The flowlines have a mean orientation of 100–116°, mean length of ~1.3 km and are parallel to ice flow. We trace the origin of these flowlines 10 km further up-glacier in Landsat imagery (Figure 2). The flowlines are apparent down-glacier for 3 km, after which they are indistinguishable within the glacier surface.

IGS, the observed supraglacial hydrological system is predominantly linear and is strongly controlled by surface crevasses and fractures. Channels that exhibit a meandering pattern are confined to areas exclusively free of crevassing, primarily within areas that experience a moderate velocity averaging at ~0.20 m d^{-1}. The supraglacial channels we observe have a mean width of 2 m and range in length up to 4 km.

Once a channelized drainage system has been established, meltwater is efficiently routed across the glacier surface either directly to the terminus or margins, or to the subglacial system via moulins. At IGS, wherever a supraglacial channel stops abruptly we assume that meltwater is either drained by a moulin (Smith et al., 2015) or forms a standalone supraglacial lake (Fitzpatrick et al., 2014).

4.3.2. Supraglacial lakes

Supraglacial lakes are either directly connected into the supraglacial network or are standalone isolated features. Supraglacial lakes tend to form in the same location every summer, being influenced by subglacial topographic depressions which express themselves in the ice surface (Echelmeyer, Clarke, & Harrison, 1991). The evolution of supraglacial lakes is dictated by a positive albedo-feedback mechanism (Sneed & Hamilton, 2007), in which the lake increases in size

due to preferential melting from increased radiation absorption of the surface water when compared to the surrounding ice (Lüthje, Pedersen, Reeh, & Greuell, 2006). We observe ~330 supraglacial lakes across the entire breadth of IGS that vary in size from 8 m^2 to 1 km^2, with >95% of the lakes being directly connected to the supraglacial network within areas of limited crevassing. These lakes follow no distinctive pattern regarding their shape or orientation to the flow direction.

4.3.3. Marginal lakes

Ice marginal lakes occur on both lateral margins of IGS, with 23 marginal lakes mapped. The lakes are constrained by marked ridges and plateaus within the topography, ranging in elevation from 370 m to 620 m, with the plateaus increasing in elevation with distance upglacier. Ice marginal lakes along the southern margin range from 700 m^2 to 0.5 km^2 in size, whereas the northern margin is dominated by the presence of a ~3.2 km^2 marginal lake (Figure 5).

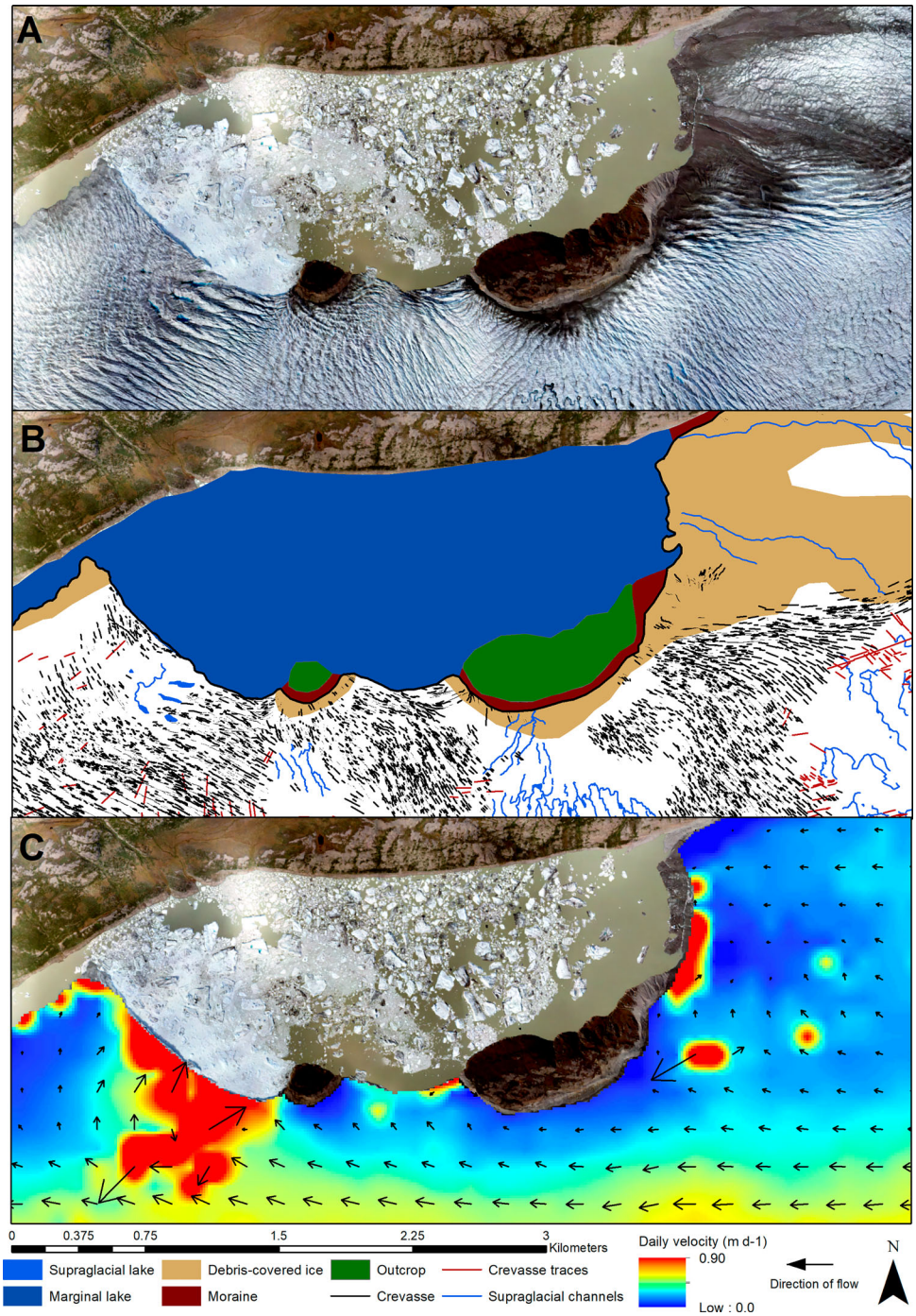

Figure 5. Digitization of the ice having contact with the northern ~3.2 km^2 marginal lake. The presence of this lake causes a dynamic flow field (C) with evolving structures (B) around the vicinity of the ice-lake interface, which is particularly apparent on the western margin. The section of ice that is in direct contact with the easterly margin of the lake is largely debris-covered and free of crevasses, suggesting that the lake is causing buoyancy induced floating ice within this region. Buoyancy induced floating of ice margins can amplify the rate of glacier retreat (Van der Veen, 2002) through influencing ice thickness and calving dynamics (Tsutaki, Nishimura, Yoshizawa, & Sugiyama, 2011).

The majority of these lakes are in direct contact with the glacier so are defined as ice-contact lakes. Marginal lakes play an important role within the glaciological environment due to their influence on both landform development (Winsemann, Brandes, & Polom, 2011) and ice flow dynamics (Diolaiuti et al., 2006).

4.3.4. Outwash plain

Glacier outwash plains, also known as sandur plains, are composed of soft, highly deformable sediments and fine stratified deposits (Aðalgeirsdóttir, Jóhannesson, Björnsson, Pálsson, & Sigurðsson, 2006) that have been worked and deposited by pro-glacial river networks. This results in a highly dynamic and variable braided river network that is evolving with seasonal and diurnal glacier discharge and sediment loads. In addition to this, the Kangerlussuaq region experiences continuous permafrost conditions (Anderson et al., 2017). This makes the sediments highly deformable, which further explains the dynamic nature of the channelized proglacial stream network. IGS has an active subglacial drainage network with two portals at the terminus of the glacier. We observe that the main portal is located at the southern end of the terminus which injects subglacial water into a large channelized hydrological system with maximum width of ~260 m. The second point of exit is on the northern end of the terminus where we observe a slow-moving heavily braided network, with a mean channel width of ~6 m.

5. Conclusion

We produced a 0.5 m resolution orthomosiac and 1.5 m resolution DEM from the application of Structure-from-Motion (SfM) photogrammetry to 3637 images obtained from three fixed-wing UAV surveys of a custom-built Skywalker X8. The imagery was used to map the structural, geomorphological and hydrological features of the tongue of Isunguata Sermia, a land-terminating outlet that drains the western sector of the GrIS, over the over the surface of the glacier in July 2015. Using this high a resolution of imagery, we were able to map the features at a scale of 1:42,000 (Main Map). We showcased how cost- and time-effective UAV technology can be used to map glacier structures, with this output then being used to better aid our understanding of glacier dynamics at both a higher spatial and temporal resolution that is currently unavailable through in-situ measurements or remotely sensed imagery. Through doing so, several research questions arise from our findings:

(1) What is the relationship between glacier velocity and the structural evolution of features throughout time?
(2) What is the driving mechanism behind crevasse formation through fracture mechanics?
(3) Are we able to predict fracture mechanics by using repeat-pass UAV imagery?

Repeat surveys would inform on the evolving stress and strain regime of the glacier as its velocity fluctuates, as shown by previous studies that have used repeat structural mapping to understand changes in glacier dynamics (e.g. Glasser & Scambos, 2008; Holt et al., 2014; King, Hambrey, Irvine-Fynn, & Holt, 2016 for example). Future studies integrating UAV imagery and structural glaciology analysis therefore show promise in answering these questions and broadening our understanding of IGS system and the dynamic records of other Greenland outlet glaciers.

Software

The DEM and orthomosiac used to create the Isunguata Sermia 1:40,000 map were produced using Agisoft PhotoScan version 1.2.5.2614. Before importing into PhotoScan, the RAW photographs collected from the July 2015 UAV surveys was converted to JPG using the Sony Image Data Converter, version 4.2.04.17270. Esri ArcGIS 10.2 was used for all structural mapping and the production of the final map.

Acknowledgements

The authors would like to thank J. Abraham, L. Thomson, O. King and M. Smith for their thorough comments and detailed suggestions that greatly improved the overall quality of both this article and the supplementary map. Alun Hubbard gratefully acknowledges a Research Professorship from the Research Council of Norway through its Centres of Excellence funding scheme grant No. 223259. Fieldwork was funded by the Dark Snow Project and NERC Project NE/G005796/1. CJ was supported by a NERC PhD Studentship.

Disclosure statement

No potential conflict of interest was reported by the authors.

References

Aðalgeirsdóttir, G., Jóhannesson, T., Björnsson, H., Pálsson, F., & Sigurðsson, O. (2006). Response of hofsjökull and southern vatnajökull, Iceland, to climate change. *Journal of Geophysical Research*, *111*, F03001. doi:10.1029/2005JF000388

Adam, W., & Knight, P. (2003). Identification of basal layer debris in ice-marginal moraines, Russell glacier, West Greenland. *Quaternary Science Reviews*, *22*(14), 1407–1414. doi:10.1016/S0277-3791(03)00079-9

Alexander, D., Davies, T., & Shulmeister, J. (2011). A steady-state mass-balance model for the Franz Josef glacier, New Zealand: Testing and application. *Geografiska Annaler. Series A: Physical Geography*, *93*(1), 41–54. doi:10.1111/j.1468-0459.2011.00003.x

Anderson, J., Saros, J., Bullard, J., Cahhon, S., McGowan, S., Bagshaw, E., … Yde, J. (2017). The Arctic in the 21st

century: Changing biogeochemical linkages across a paraglacial landscape of Greenland. *BioScience*, *67*(1), 118–133. doi:10.1093/biosci/biw158

Benn, D., & Evans, D. (2010). *Glaciers & glaciation: Glacier dynamics*. Abingdon: Hodder Education.

Bhardwaj, A., Sam, L., Martín-torres, F., & Kumar, R. (2016). Remote sensing of environment UAVs as remote sensing platform in glaciology : present applications and future prospects. *Remote Sensing of Environment*, *175*, 196–204. doi:10.1016/j.rse.2015.12.029

Cathles, L., Abbot, D., Bassis, J., & MacAyeal, D. (2011). Modeling surface-roughness/solar-ablation feedback: Application to small-scale surface channels and crevasses of the Greenland Ice Sheet. *Annals of Glaciology*, *52*(59), 99–108. doi:10.3189/172756411799096268

Colgan, W., Rajaram, H., Abdalati, W., Mccutchan, C., Mottram, R., Moussavi, M., & Grigsby, S. (2016). Glacier crevasses: Observations, models and mass balance implications. *Reviews of Geophysics*, *54*, doi:10.1002/2015RG000504

Diolaiuti, G., Citterio, M., Carnielli, T., D'Agata, C., Kirkbride, M., & Smiraglia, C. (2006). Rates, processes and morphology of freshwater calving at Miage Glacier (Italian Alps). *Hydrological Processes*, *20*(10), 2233–2244. doi:10.1002/hyp.6198

Echelmeyer, K., Clarke, T., & Harrison, W. (1991). Surficial glaciology of Jakobshavns Isbræ, West Greenland: Part I. Surface morphology. *Journal of Glaciology*, *37*(127), 15.

Fitzpatrick, A., Hubbard, A., Box, J., Quincey, D., van As, D., Mikkelsen, A., … Jones, G. (2014). A decade (2002–2012) of supraglacial lake volume estimates across Russell Glacier, West Greenland. *The Cryosphere*, *8*, 107–121. doi:10.5194/tc-8-107-2014

Fitzpatrick, A., Hubbard, A., Joughin, I., Quincey, D., Van As, D., Mikkelsen, A., … Jones, G. (2013). Ice flow dynamics and surface meltwater flux at a land-terminating sector of the Greenland Ice Sheet. *Journal of Glaciology*, *59*(216), 687–696. doi:10.3189/2013JoG12J143

Forster, R., Box, J., van den Broeke, M., Miège, C., Burgess, E., van Angelen, J., … McConnell, J. (2014). Extensive liquid meltwater storage in firn within the Greenland Ice Sheet. *Nature Geoscience*, *7*(2), 1–4. doi:10.1038/ngeo2043

Gindraux, S., Boesch, R., & Farinotti, D. (2016). Accuracy assessment of digital surface models from unmanned aerial vehicles' imagery on glaciers. *Remote Sensing*, *9*(3), 186. doi:10.3390/rs9020186

Glasser, N., & Gudmundsson, G. (2012). Longitudinal surface structures (flowstripes) on Antarctic glaciers. *Cryosphere*, *6*(2), 383–391. doi:10.5194/tc-6-383-2012

Glasser, N., Jennings, S., Hambrey, M., & Hubbard, B. (2015). Origin and dynamic significance of longitudinal structures ('flow stripes') in the Antarctic Ice Sheet. *Earth Surface Dynamics*, *3*(2), 239–249. doi:10.5194/esurf-3-239-2015

Glasser, N., & Scambos, T. (2008). A structural glaciological analysis of the Larsen B ice-shelf collapse. *Journal of Glaciology*, *54*(184), 3–16.

Goodsell, B., Hambrey, M., & Glasser, N. (2002). Formation of band ogives and associated structures at Bas Glacier d'Arolla, Valais, Switzerland. *Journal of Glaciology*, *48*(161), 287–300. doi:10.3189/172756502781831494

Hambrey, M., & Lawson, W. (2000). Structural styles and deformation fields in glaciers: A review. *Geological Society, London, Special Publications*, *176*(1), 59–83. doi:10.1144/gsl.sp.2000.176.01.06

Hambrey, M., & Muller, F. (1978). Structures and ice deformation in the White Glacier, Axel Heiberg Island, northwest territories. *Journal of Glaciology*, *20*(82), 41–66.

Harrington, J., Humphrey, N., & Harper, J. (2015). Temperature distribution and thermal anomalies along a flowline of the Greenland Ice Sheet. *Annals of Glaciology*, *56*(70), 98–104. doi:10.3189/2015AoG70A945

Holdsworth, G. (1969). An examination and analysis of the formation of transverse crevasses, Kaskawulsh Glacier. *Icefield Ranges Research Projects, Scientific Results*, *1*(16), 109–126.

Holt, T., Glasser, N., Fricker, H., Padman, L., Luckman, A., King, O., … Siegfried, M. (2014). The structural and dynamic responses of Stange Ice Shelf to recent environmental change. *Antarctic Science*, *26*(6), 646–660. doi:10.1017/S095410201400039X

Holt, T., Glasser, N., Quincey, D., & Siegfried, M. (2013). Speedup and fracturing of George VI Ice Shelf, Antarctic Peninsula. *Cryosphere*, *7*(3), 797–816. doi:10.5194/tc-7-797-2013

Howat, I., Negrete, A., & Smith, B. (2014). The Greenland Ice Mapping Project (GIMP) land classification and surface elevation data sets. *The Cryosphere*, *8*(4), 1509–1518. doi:10.5194/tc-8-1509-2014

Hubbard, A., Blatter, H., Nienow, P., Mair, D., & Hubbard, B. (1998). Comparison of a three-dimensional model for glacier flow with field data from Haut Glacier d' Arolla, Switzerland. *Journal of Glaciology*, *44*(147), 368–378. doi:10.3198/1998JoG44-147-368-378

Hulbe, C., LeDoux, C., & Cruikshank, K. (2010). Propagation of long fractures in the Ronne Ice Shelf, Antarctica, investigated using a numerical model of fracture propagation. *Journal of Glaciology*, *56*(197), 459–472. doi:10.3189/002214310792447743

King, O., Hambrey, M., Irvine-Fynn, T., & Holt, T. (2016). The structural, geometric and volumetric changes of a polythermal Arctic glacier during a surge cycle: Comfortlessbreen, Svalbard. *Earth Surface Processes and Landforms*, *41*, 162–177. doi:10.1002/esp.3796

Lindbäck, K., Pettersson, R., Doyle, S., Helanow, C., Jansson, P., Kristensen, S., … Hubbard, A. (2014). High-resolution ice thickness and bed topography of a land-terminating section of the Greenland Ice Sheet. *Earth System Science Data*, *6*(2), 331–338. doi:10.5194/essd-6-331-2014

Lindbäck, K., Pettersson, R., Hubbard, A., Doyle, S., van As, D., Mikkelsen, A., & Fitzpatrick, A. (2015). Subglacial water drainage, storage, and piracy beneath the Greenland Ice Sheet. *Geophysical Research Letters*, *42*(18), 7606–7614. doi:10.1002/2015GL065393

Lüthje, M., Pedersen, L., Reeh, N., & Greuell, W. (2006). Modelling the evolution of supraglacial lakes on the west Greenland ice-sheet margin. *Journal of Glaciology*, *52*(179), 608–618. doi:10.3189/172756506781828386

Marston, R. (1983). Supraglacial stream dynamics on the Juneau Icefield. *Annals of the Association of American Geographers*, *73*(4), 597–608. doi:10.1111/j.1467-8306.1983.tb01861.x

Meierbachtol, T., Harper, J., & Johnson, J. (2016). Force balance along Isunnguata Sermia, West Greenland. *Frontiers in Earth Science*, *4*(87), doi:10.3389/feart.2016.00087

Messerli, A., & Grinsted, A. (2015). Image georectification and feature tracking toolbox: ImGRAFT. *Geoscientific instrumentation. Methods and Data Systems*, *4*(1), 23–34. doi:10.5194/gi-4-23-2015

Mohammed, N., Ghazi, A., & Mustafa, H. (2013). Positional accuracy testing of Google Earth. *International Journal of Multidisciplinary Sciences and Engineering*, *4*(6), 6–9.

Nakawo, M., Iwata, S., & Yoshida, M. (1986). Processes which distribute supraglacial debris on the Khumbu Glacier, Nepal Himalaya. *Annals of Glaciology*, *8*(1977), 129–131. Retrieved from http://www.igsoc.org:8080/annals/8/igs_annals_vol08_year1985_pg129-131.pdf

Oerlemans, J., Giesen, R., & Van Den Broeke, M. (2009). Retreating alpine glaciers: Increased melt rates due to accumulation of dust (Vadret da Morteratsch, Switzerland. *Journal of Glaciology*, *55*(192), 729–736. doi:10.3189/002214309789470969

Rippin, D., Pomfret, A., & King, N. (2015). High resolution mapping of supraglacial drainage pathways reveals link between micro-channel drainage density, surface roughness and surface reflectance. *Earth Surface Processes and Landforms*, *40*, 1279–1290. doi:10.1002/esp.3719

Ryan, J., Hubbard, A., Box, J., Brough, S., Cameron, K., Cook, J., … Snooke, N. (2017). Derivation of high spatial resolution albedo from UAV digital imagery: Application over the Greenland Ice Sheet. *Frontiers in Earth Science*, *5*(40). doi:10.3389/feart.2017.00040

Ryan, J., Hubbard, A., Box, J., Todd, J., Christoffersen, P., Carr, J., … Snooke, N. (2015). UAV photogrammetry and structure from motion to assess calving dynamics at store glacier, a large outlet draining the Greenland Ice Sheet. *Cryosphere*, *9*(1), 1–11. http://doi.org/10.5194/tc-9-1-2015

Ryan, J., Hubbard, A., Stibal, M., Box, J., & Team., D. S. P. (2016). Attribution of Greenland's ablating ice surfaces on ice sheet albedo using unmanned aerial systems. *The Cryosphere Discussions*, doi:10.5194/tc-2016-204

Smith, L., Chu, V., Yang, K., Gleason, C., Pitcher, L., Rennermalm, A., … Balog, J. (2015). Efficient meltwater drainage through supraglacial streams and rivers on the southwest Greenland Ice Sheet. *Proceedings of the National Academy of Sciences of the United States of America*, *112* (4), 1001–1006. http://doi.org/10.1073/pnas.1413024112

Smith, M., Carrivick, J., & Quincey, D. (2015). Structure from motion photogrammetry in physical geography. *Progress in Physical Geography*, *40*(2), 247–275. doi:10.1177/0309133315615805

Sneed, W., & Hamilton, G. (2007). Evolution of melt pond volume on the surface of the Greenland Ice Sheet. *Geophysical Research Letters*, *34*(3), 4–7. doi:10.1029/2006GL028697

Thomson, L., & Copland, L. (2016). White glacier 2014, Axel Heiberg Island, Nunavut: Mapped using structure from motion methods. *Journal of Maps*, *12*(5), 1063–1071. doi:10.1080/17445647.2015.1124057

Tonkin, T., Midgley, N., Graham, D., & Labadz, J. (2014). The potential of small unmanned aircraft systems and structure-from-motion for topographic surveys: A test of emerging integrated approaches at Cwm Idwal, North Wales. *Geomorphology*, *226*, 35–43. doi:10.1016/j.geomorph.2014.07.021

Tsutaki, S., Nishimura, D., Yoshizawa, T., & Sugiyama, S. (2011). Changes in glacier dynamics under the influence of proglacial lake formation in Rhonegletscher, Switzerland. *Annals of Glaciology*, *52*(58), 31–36. doi:10.3189/172756411797252194

van As, D., Hubbard, A., Hasholt, B., Mikkelsen, A., van den Broeke, M., & Fausto, R. (2012). Large surface meltwater discharge from the Kangerlussuaq sector of the Greenland Ice Sheet during the record-warm year 2010 explained by detailed energy balance observations. *The Cryosphere*, *6*, 199–209. doi:10.5194/tc-6-199-2012

Van der Veen, C. (1999). Crevasses on glaciers. *Polar Geography*, *23*(3), 1–33. doi:10.1080/10889379909377677

Van der Veen, C. (2002). Calving glaciers. *Progress in Physical Geography*, *26*(1), 96–122. doi:10.1191/0309133302pp327ra

Vaughan, D. (1993). Relating the occurrence of crevasses to surface strain rates. *Journal of Glaciology*, *39*(132), 255–266. doi:10.1016/0148-9062(94)90888-5

Vornberger, P. L., & Whillans, I. M. (1990). Crevasse deformation and examples from Ice stream B, Antarctica. *Journal of Glaciology*, *36*(122), 3–10.

Vornberger, P. L., & Whillans, I. M. (1986). Surface features of Ice Stream B, Marie Byrd Land, West Antarctica. *Annals of Glaciology*, *8*, 168–170.

Winsemann, J., Brandes, C., & Polom, U. (2011). Response of a proglacial delta to rapid high-amplitude lake-level change: An integration of outcrop data and high-resolution shear wave seismics. *Basin Research*, *23*(1), 22–52. doi:10.1111/j.1365-2117.2010.00465.x

Wright, P., Harper, J., Humphrey, N., & Meierbachtol, T. (2016). Journal of geophysical research : earth surface Greenland Ice Sheet: Implications for hydraulic potential. *Journal of Geophysical Research: Earth Surface*, *121*, 1134–1147. doi:10.1002/2016JF003819

Yang, K., Li, M., Liu, Y., Chng, L., Huang, Q., & Chen, Y. (2015). River detection in remotely sensed imagery using Gabor filtering and path opening. *Remote Sensing*, *7*(7), 8779–8802. doi:10.3390/rs70708779